33RD INTERNATIONAL COSMIC RAY CONFERENCE, RIO DE JANEIRO 2013
THE ASTROPARTICLE PHYSICS CONFERENCE

ICRC 2013

The Multiple Muon Charge Ratio in MINOS

C. M. CASTROMONTE[1], R. A. GOMES[1], FOR THE MINOS COLLABORATION.

[1] *Instituto de Física, Universidade Federal de Goiás, CP 131, 74001-970, Goiânia, GO, Brazil*

cesarc@if.ufg.br

Abstract: The MINOS Far Detector is a magnetized planar steel-scintillator detector situated underground at depth of 2070 mwe. A small fraction of the cosmic ray muons observed in the MINOS FD contain multiple muons. These events on average are expected to have originated from either higher mass primaries, or higher energy protons than their single muon counterparts. Using the complete MINOS atmospheric data set we will present the first measurement of the multiple muon events charge ratio $R_\mu = N_{\mu^+}/N_{\mu^-}$. Systematic uncertainties on the charge ratio were minimized by utilizing data collected with both forward and reversed magnetic field running.

Keywords: MINOS, cosmic rays, multiple muons.

1 Introduction

Atmospheric muons are produced when primary cosmic ray nuclei interact near the top of the atmosphere to produce hadronic showers which contain pions and kaons. These secondary mesons can either interact in further collisions in the atmosphere or decay to produce atmospheric muons. Since the majority of primary cosmic rays are protons, there is an excess of positively charged mesons in the showers, and consequently, the atmospheric muon charge ratio $R_\mu = N_{\mu^+}/N_{\mu^-}$, defined as the number of positive over negative muons, is larger than unity. It's expected that heavier elements become a more important component of cosmic ray primaries as the energy increases. This increasingly heavy composition would decrease the ratio of primary protons to neutrons, which in turn, would decrease the muon charge ratio. With careful measurements of the muon charge ratio in the cosmic rays, models of the interactions of cosmic rays in the atmosphere can be improved.

A multiple muon event is one in which two or more nearly parallel, time-coincident muon tracks are observed in the detector. At high energies, massive primaries generate more high-energy muons per event than proton primaries of the same total energy. This is because the initial parent meson (predominantly pion) particle multiplicities are larger from the more massive primary, and the atmosphere is more favorable to pion decay versus interaction early in the cascade development. In addition, the point of first interaction of the heavy primary is likely to be higher in the atmosphere than for the proton primary due to the larger cross section of the heavy nucleus-air interactions.

Previous single muon charge ratio measurements performed by MINOS (Near Detector) [1], L3 + C [2], BessTEV [3], CosmoALEPH [4] and CMS [5] at energies at the surface level E_μ ranging from a few hundred Mev to 500 GeV are consistent with the 2001 world average of $1.268 \pm [0.008 \pm 0.0002 \frac{E_\mu}{\mathrm{GeV}}]$ [6]. MINOS (Far Detector) [7] and OPERA [8] also reported, at TeV surface energies, a higher value for the muon charge ratio (≈ 1.37). For the multiple muon charge ratio, OPERA reported the values of 1.23 ± 0.06 [8] (2010) and 1.18 ± 0.03 [9] (2013).

In this paper we present a measurement of the atmospheric muon charge ratio using a sample of multiple muons recorded by the MINOS Far Detector.

2 The MINOS Far Detector

The MINOS Far Detector is a magnetized planar steel-scintillator detector located at a depth of 2070 mwe in the Soudan Underground Laboratory in an iron mine in northern Minnesota (latitude 47.820 27° N and longitude 92.241 41° W). The detector contains 486 octagonal steel planes, each 2.54 cm thick, interleaved with 484 planes of 1 cm thick extruded polystyrene scintillator strips at a 5.94 cm pitch. Each scintillator plane has 192 strips of width 4.1 cm. The length of each strip depends on its position in the plane and varies between 3.4 and 8.0 m. The scintillator strips in alternating detector planes are oriented at $\pm 45°$ to the vertical. The modular detector consists of two supermodules (SM) separated by a gap of 1.1 m. Scintillation light is collected by wavelength shifting (WLS) plastic fibers embedded within the scintillator strips. The WLS fibers are coupled to clear optical fibers at both ends of a strip and are read out using 16-pixel multianode phototmultiplier tubes (PMTs). The signals from eight strips, each one of which is separated by approximately 1 m within the same plane, are optically summed and read out by a single PMT pixel. The fibers summed on each pixel are different for the two sides of the detector, which enables the resulting eightfold ambiguity to be resolved for single particle events. For all other types of events, ambiguities are effectively resolved using additional information from timing and event topology.

In order to measure the momentum of muons traversing the detector, the steel has been magnetized into a toroidal field configuration. The field varies in strength from 1.8 T near the magnetic coil to almost 1 T near the edges. A muon is "focused" when the magnetic field steers it toward the center of the detector and "defocused" when directed away from the center. The MINOS magnetic field was designed to focus negatively charged particles coming from the south (i.e., μ^- resulting from ν_μ interactions in the detector from neutrinos originating in the Fermilab NuMI beam) toward the center of the detector. This magnetic field orientation will be referred as data forward ("DF") configuration. MINOS has a second field orientation, data reverse ("DR") configuration, in which the coil current is reversed and μ^+ from the south are focused into the detector.

Information regarding the data acquisition and trigger

systems can be found in [10]. The detector calibration has been described in [11]. More detailed detector information can be found in [12].

3 Data Analysis

The multiple muon sample reported in this paper was recorded between August 2003 and April 2012. During the data taking period, the detector run with both the DF and DR magnetic field configurations.

3.1 Event selection

A selection criteria (or cuts) have been chosen to ensure the highest quality of data. The first stage of the event selection is to identify and remove periods of data associated with detector hardware problems. The criteria which define bad runs are described in [13]. Most of the cuts used to select the sample for this analysis are similar to those used in previous Far Detector muon analysis [7, 14]. For a multiple muon event it was required that tracks in the event to be downward-going and to satisfy a "parallel" cut, i.e., for each muon track there is an angular separation of less than 5° from at least one other muon in the group. If at least a pair of tracks in the event satisfies this cut, all the muons in that event are considered in the calculation of the charge ratio. This cut is meant to ensure that at least two tracks are correlated. A summary of the cuts applied and their selection efficiencies are shown in Table 1.

3.1.1 Charge-sign quality cuts

Two selection variables are used to further increase the degree of confidence in the assigned curvature and charge sign of the tracks. The Kalman filter [15] technique used in the track curvature fitting involves a series of recursive matrix manipulations to specify the trajectory of the particle as well as the ratio of its charge to its momentum (q/p). It also provides an uncertainty $\sigma(q/p)$ on the measured value of q/p. The first charge sign quality cut is based on the charge-sign significance, $(q/p)/\sigma(q/p)$, determined by the track fitter. The second cut variable BdL is defined as

$$BdL \equiv \int_{\text{beg}}^{\text{end}} B_{\text{perp}}(r)dL \qquad (1)$$

where $B_{\text{perp}}(r) = |\vec{B}(r) \times \vec{n}|$ is the component of the magnetic field perpendicular to the track direction $\vec{n}$ at a given point along the track path, r is the distance from the detector center axis, dL is the differential pathlength element along the track, *beg* is the point at which the muon enters the detector, and *end* is the point at which it either exits the detector or stops in the detector. The BdL cut ensures that the magnitude of the bending due to curvature is larger than apparent bending due to multiple scattering.

Figures 1 and 2 show the multiple muon charge ratio as a function of $(q/p)/\sigma(q/p)$ and of BdL respectively, for data collected in both magnetic field orientations. The charge ratio for data collected in a single magnetic field orientation is defined as the ratio of positive to negative muons collected only in that orientation. The figures also show systematic differences in the charge ratio measurements between forward and and reverse magnetic field running. These differences come from acceptance effects due to the magnetic field, detector asymmetry, and detector alignment errors. To remove these biases, data taken in the two field orientations were combined by calculating a geometric mean (GM) between both data sets. This procedure will be discussed in the next section.

For the charge-sign significance, it was required $(q/p)/\sigma(q/p) > 3$. Above this value the charge ratio tends to be asymptotically flat, suggesting that the charge sign and momentum are well-fit. As $(q/p)/\sigma(q/p)$ tends to zero, the charge sign determined by the fitter becomes less reliable. Low values of the $(q/p)/\sigma(q/p)$ indicates that the fitter picks the two charge signs with equal probability and the measured charge-sign ratio tends to unity. Events with low values of the charge-sign significance are typically high momentum tracks (> 100 GeV/c) that traverse the detector in such a way as to bend only slightly in the magnetic field.

It was also required $BdL > 5$ T m. For low values of BdL, the measured charge ratio approaches to one, as expected in the case of random charge determination. As the integrated magnetic field increases, the charge ratio increases to a plateau value where the charge misidentification is suppressed. The BdL cut was chosen as the value where the plateau is reached. Above this value the charge ratio as function of BdL is consistent with being constant.

Superposed onto both, the $(q/p)/\sigma(q/p)$ and BdL data plots, there is a fit of the combined distributions to a constant charge ratio. In both cases it was obtained a muon charge ratio of 1.08 ± 0.01.

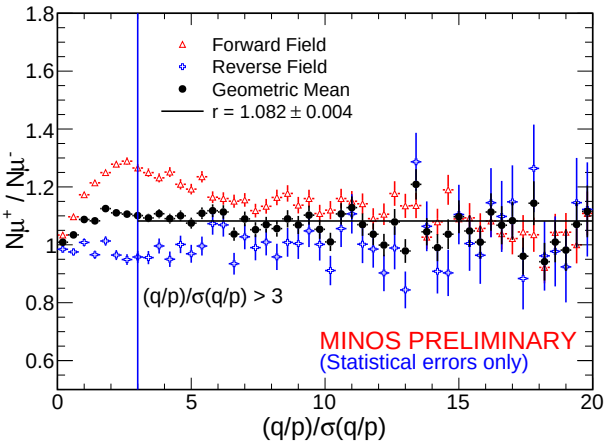

Fig. 1: Charge ratio for reconstructed multiple muon tracks as a function of $(q/p)/\sigma(q/p)$ after all selection cuts and requiring that $BdL > 5$ T m. The vertical line is the threshold value used in the charge-sign quality selection. Data points show only statistical errors. Superposed is the fit of the combined distribution (geometric mean) to a constant charge ratio N_{μ^+}/N_{μ^-}.

Events which have passed all the cuts summarized in Table 1 are used in the calculation of the multiple muon charge ratio described in the next section.

3.1.2 Measurement of the Multiple Muon charge ratio underground

In this section we determine the muon charge ratio, $R_\mu = N_{\mu^+}/N_{\mu^-}$, as a function of the muon multiplicity.

As shown in the previous section, magnetic field effects in the Far Detector introduce a bias in the charge ratio when it is calculated using only data from a single magnetic field orientation. A method to cancel geometrical acceptance effects and alignment errors is discussed in [7, 16]. Two independent equations for the charge ratio, r_a and r_b, can

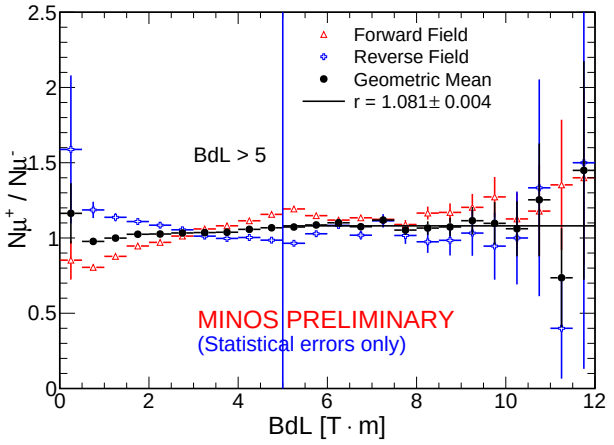

Fig. 2: Charge ratio for reconstructed multiple muon tracks as a function of *BdL* after all selection cuts and requiring that $(q/p)/\sigma(q/p) > 3$. The vertical line is the threshold value used in the charge-sign quality selection. Data points show only statistical errors. Superposed is the fit of the combined distribution (geometric mean) to a constant charge ratio N_{μ^+}/N_{μ^-}.

be constructed in which the magnetic field effects cancel. These live time corrected ratios are

$$r_a = (N^{\mu^+}_{\rm DF}/\tau_{\rm DF})/(N^{\mu^-}_{\rm DR}/\tau_{\rm DR}) \quad (2)$$

and

$$r_b = (N^{\mu^+}_{\rm DR}/\tau_{\rm DR})/(N^{\mu^-}_{\rm DF}/\tau_{\rm DF}) \quad (3)$$

The geometric mean (GM) of r_a and r_b provides a measurement of the charge ratio, R_μ, in which magnetic field effects, alignment errors and live time biases cancel

$$R_\mu = [r_a \times r_b]^{1/2} = \left[\left(\frac{N^{\mu^+}_{\rm DF}}{N^{\mu^-}_{\rm DF}}\right) \times \left(\frac{N^{\mu^+}_{\rm DR}}{N^{\mu^-}_{\rm DR}}\right)\right]^{1/2} \quad (4)$$

Figures 1 and 2 illustrate very well that the apparent significant bias in the charge ratio in a single field orientation data set is strongly suppressed in the geometric mean.

After all the cuts shown in Table 1 have been applied we obtain a final sample of **393144** muons. Figure 3 and Table 2 show the calculated muon charge ratio as a function of the muon multiplicity. The errors shown in both are only statistical.

By fitting the combined data set (GM) in Figure 3 to a constant charge ratio we obtain a value of $N_{\mu^+}/N_{\mu^-} = 1.080 \pm 0.004(stat)$, for muon multiplicities between 2 and 7.

4 Summary

A preliminary measured of the atmospheric muon charge ratio $R_\mu = N_{\mu^+}/N_{\mu^-}$ as a function of the muon multiplicity was performed using the full MINOS Far Detector atmospheric data set.

For muon multiplicities between 2 and 7, we obtain a charge ratio value

$$N_{\mu^+}/N_{\mu^-} = 1.080 \pm 0.004(stat)$$

Cuts	Data selection efficiency
# muons before cuts	8.35×10^6 (100%)
Preselection	
magnet coil status	8.06×10^6 (96.5%)
one well reconst. track	7.66×10^6 (91.7%)
Physics cuts	
parallel tracks ($< 5°$)	7.31×10^6 (87.5%)
at least 20 planes	5.88×10^6 (70.5%)
> 2 m track length	5.87×10^6 (70.3%)
downward-going track	5.86×10^6 (70.2%)
XY track vtx. pos. > 0.5 m	5.85×10^6 (70.0%)
Charge-sign quality	
$(q/p)/\sigma(q/p) > 3$	1.10×10^6 (16.7%)
$BdL > 5$	3.93×10^5 (4.7%)

Table 1: Summary of the cuts applied. Each row shows the total number of muons remaining after all the applied cuts; in parenthesis, the percentage of muons remaining.

Mult.	DF	DR	GM
2	1.182 ± 0.005	1.021 ± 0.009	$\mathbf{1.098 \pm 0.005}$
3	1.120 ± 0.010	0.963 ± 0.017	$\mathbf{1.039 \pm 0.010}$
4	1.119 ± 0.016	0.978 ± 0.028	$\mathbf{1.046 \pm 0.017}$
5	1.146 ± 0.026	0.876 ± 0.041	$\mathbf{1.002 \pm 0.026}$
6	1.115 ± 0.040	0.962 ± 0.071	$\mathbf{1.036 \pm 0.042}$
7	1.127 ± 0.067	0.898 ± 0.101	$\mathbf{1.006 \pm 0.064}$

Table 2: Summary of the measured muon charge ratio as a function of muon multiplicity for DF, DR and combined (GM) data sets. The errors shown in the charge ratios are only statistical.

No efficiency corrections or systematic errors have been included in the results as this analysis is currently underway.

Acknowledgment: This work was supported by the U.S. DOE, the United Kingdom STFC, the U.S. NSF, the State and University of Minnesota, the University of Athens, Greece, and Brazils CAPES and REUNI-UFG. We gratefully acknowledge the Minnesota Department of Natural Resources and the crew of Soudan Underground Laboratory.

References

[1] P. Adamson et al. (MINOS Collaboration), Phys. Rev. D 83, 032011 (2011).
[2] P. Achard et al. (L3 Collaboration), Phys. Lett. B 598, 15 (2004).
[3] S. Haino et al., Phys. Lett. B 594, 35 (2004).
[4] D. Zimmermann et al., Nucl. Instrum. Meth. A 525, 141 (2004).
[5] V. Khachatryan et al. (CMS Collaboration), Phys. Lett. B 692, 83 (2010).
[6] T. Hebbeker and C. Timmermans, Astropart. Phys. 18, 107 (2002).
[7] P. Adamson et al. (MINOS Collaboration), Phys. Rev. D 76, 052003 (2007).
[8] N. Agafonova et al. (OPERA Collaboration), Eur. Phys. J. C 67, 25 (2010).

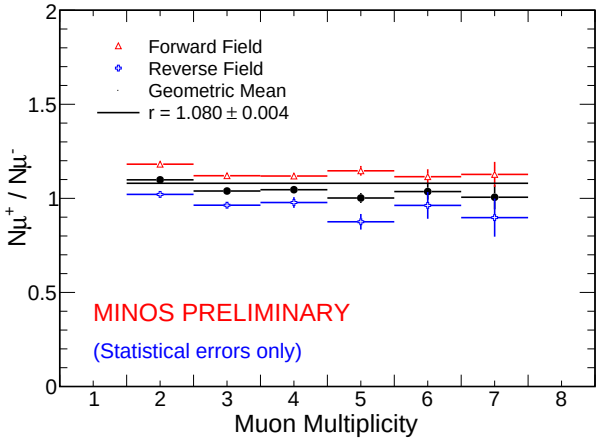

Fig. 3: The measured muon charge ratio as a function of the muon multiplicity for the DF data set, DR data set and combined data set (GM). The GM distribution shows the charge ratio in which magnetic field effects, alignment errors and live time biases cancel. Data points show only statistical errors. Superposed is the fit of the GM distribution to a constant charge ratio N_{μ^+}/N_{μ^-}, for muon multiplicities between 2 and 7.

[9] N. Mauri et al. (OPERA Collaboration), LHC-CR Workshop: Results and prospects of forward physics at the LHC, (2013).
[10] P. Adamson et al. (MINOS Collaboration), Phys. Rev. D 73, 072002 (2006).
[11] P. Adamson et al. (MINOS Collaboration), MINOS Technical Design Report, Fermilab Note MINOS- 337, 1998.
[12] D.G. Michael et al. (MINOS Collaboration), Nucl. Instrum. Meth. A 596, 190-228 (2008).
[13] A. Blake, Ph.D. thesis, Cambridge University, 2005.
[14] P. Adamson et al. (MINOS Collaboration), Phys. Rev. D 81, 012001 (2010).
[15] R. Fruhwirth, Nucl. Instrum. Meth. A 262, 444 (1987).
[16] S. Matsuno et al., Phys. Rev. D 29, 1 (1984).